Thin-Walled Structures 117 (2017) 190–198

Contents lists available at ScienceDirect

Thin-Walled Structures

journal homepage: www.elsevier.com/locate/tws

Full length article

Crushing analysis and multiobjective optimization design for rectangular unequal triple-cell tubes subjected to axial loading

Wen Shen[a], Xianguang Gu[a,b,*], Ping Jiang[a], Jinfang Hu[a], Xiaojiang Lv[c], Lijun Qian[a]

[a] School of Automobile and Traffic engineering, Hefei University of Technology, 230009 Hefei, Anhui, PR China
[b] Key Laboratory of Advanced Manufacture Technology for Automobile Parts (Chongqing University of Technology), Ministry of Education, Chongqing 400054, PR China
[c] Zhejiang Key Laboratory of Automobile Safety Technology, Geely Automobile Research Institute, Hangzhou, Zhejiang 311228, PR China

ARTICLE INFO

Keywords:
Triple-cell section
Axial crushing
Theoretical prediction
Multiobjective optimization

ABSTRACT

Multi-cell thin-walled tubes have proven to be better in energy absorption than plain square tubes subjected to axial compression. Therefore, square multi-cell structures have been extensively utilized as energy absorbers in automobiles. This paper provides an investigation on the crashworthiness of rectangular single-, double- and triple-cell columns under axial loading and an optimization design of rectangular unequal triple-cell tubes. First, a theoretical solution is derived for the mean crushing force (MCF) of tubes with unequal triple-cell configuration. Second, quasi-static crushing experiments and finite element analyses (FEA) are conducted on single-, double- and unequal triple-cell columns. Theoretical predictions compare well with experimental and numerical data, and all results show that the triple-cell tubes exhibit the best crashworthiness among all the samples. Third, in order to study effects of wall thickness distribution and the layout of internal ribs on crashing behavior, multiobjective optimization design is implemented combining Radial Basis Function (RBF) model with Non-dominant sorting Genetic Algorithm II (NSGA-II). The optimal solution obtained from Pareto frontier indicates that unequal triple-cell tube with appropriate thickness distribution and arrangement of internal ribs is superior in energy absorption to initial design.

1. Introduction

Thin-walled metal tubes have been widely used in vehicles serving as energy absorbers in the process of crash. For instance, crash boxes in automotive body-in-white (BIW) are always metal thin-walled structures that can absorb kinetic energy through plastic deformation when collision occurs. Recently, a great number of studies have been carried out to explore the crashworthiness of metal tubes under axial load [1–4]. Among all research directions, structural investigation has caught the attention of many scholars, and as a result a wide range of sectional configurations have been investigated aiming to find out structures with better energy absorbing ability and lower weight, for instance, the circular, square, polygonal tubes and their tapered variations [5–10].

Square metal tubes are one of the most commonly used among all kinds of sectional configurations. To improve the crashworthiness of square tubes, numerous studies have been carried out exploring square structures that have been divided axially into several cells by adding internal ribs. For example, Chen and Wierzbichi investigated square double-cell and triple-cell tubes and summarized formulae for predicting mean crushing force (MCF) [11]. Zhang et al. studied square multi-cell columns numerically and proposed a more convenient formula to predict MCF of multi-cell tubes [12]. Hou and Li investigated square tubes of single-, double-, triple- and quadruple-cell in aspect of crashworthiness. Single- and multi-objective optimizations were performed in terms of sectional width and wall thickness in Hou and Li's study. It was found that sectional width and wall thickness could affect crashing performance notably [13]. Zhang et al. studied crashing behaviors of multi-cell tubes and used constitutive element method to predict the crush resistance [14]. Previous studies have shown that multi-cell square tubes are more efficient in energy absorption than plain square columns and worth paying great efforts.

It should be noted that most multi-cell tubes were fabricated with uniform wall thicknesses and cell layouts, indicating that these thin-walled columns did not take full advantage of their material and structural advantages for the best crashworthiness. There have been some publications dealing with this issue to some extent. For example, Alavinia and Parsapour explored 3×3 square tubes of unequal-celled section and revised Zhang's [12] formula for predicting MCF of unequal multi-cell tubes [15]. It was found that unequal multi-cell tubes are

* Corresponding author at: School of Automobile and Traffic engineering, Hefei University of Technology, 230009 Hefei, Anhui, PR China.
E-mail address: gxghfut@163.com (X. Gu).

http://dx.doi.org/10.1016/j.tws.2017.04.018
Received 24 January 2017; Received in revised form 26 March 2017; Accepted 14 April 2017

superior to their uniform counterparts in terms of energy absorption. Nevertheless, many problems remain unsolved, for instance, how different thicknesses distribution and arrangements of cells lead to different crashworthiness outcomes. Therefore, there is still a need to further design multi-cell tubes for better crashing performance. To address this complicated design issue, optimization design technique needs to be employed to present an optimal solution. A number of researchers have applied multiobjective optimization technique in current crashworthiness design and acquired reasonable conclusions, e.g. Sun et al. [16], Gu et al. [17], Hou et al. [18], and Costas et al. [19]. According to these earlier studies, it can be noted that the optimization method has proven accurate and less time-consuming in non-linear design tasks.

This paper offers a study on crashworthiness of three different rectangular columns under axial loading and optimization design of rectangular unequal triple-cell tubes. In this paper, rectangular tubes are all made of aluminum alloy with single-cell, double-cell and unequal triple-cell sections. Firstly, an improved formula for predicting axial MCF of rectangular unequal-cell tubes is derivated based on Alavinia's [15] formula. The finite element analysis (FEA) models for tubes with three kinds of different sections are then constructed by FEA code LS-DYNA. Results obtained from quasi-static simulations are verified against data from experiments and predictions. Thirdly, a system methodology, including design of experiments (DOE), radial basis function (RBF) and Non-dominated sorting genetic algorithm II (NSGA-II), is applied to conduct multiobjective optimization design. In optimization procedure, thicknesses of each plate and the arrangement of internal ribs are considered as variables. The optimal solution obtained from Pareto sets is finally validated with numerical data.

2. Evaluation criteria

To evaluate the crashworthiness quantitatively, several criteria are first introduced in this study, namely peak crushing force (PCF), mean crushing force (MCF), crushing force efficiency (CFE), energy absorption (EA) and specific energy absorption (SEA). The PCF is the first maximal value in a Force-Displacement curve. The MCF is obtained mathematically as:

$$MCF = \frac{1}{d}\int_0^d F(\delta)d\delta \tag{1}$$

where d denotes total crushing deformation; $F(\delta)$ is the instantaneous crushing force. Crushing force efficiency is a ratio of the average crushing force to the initial peak force:

$$CFE = \frac{MCF}{PCF} \tag{2}$$

The energy absorption is the total energy dissipated in plastic deformation. The specific energy absorption is defined as a ratio of the energy absorption to the weight of the tube.

$$SEA = \frac{EA}{W} \tag{3}$$

where W is the mass of specimen. Generally, when a vehicle collision occurs, MCF and PCF need to be low for occupant protection while high SEA is desirable for good energy absorption.

3. Theoretical solutions

3.1. Background

It can be achieved to calculate MCF by using analytical methods [21,22] and there have been several theoretical solutions for predicting MCF of square tubes under axial load. Wierzbicki et al. [21,22] proposed a formula for calculating MCF as:

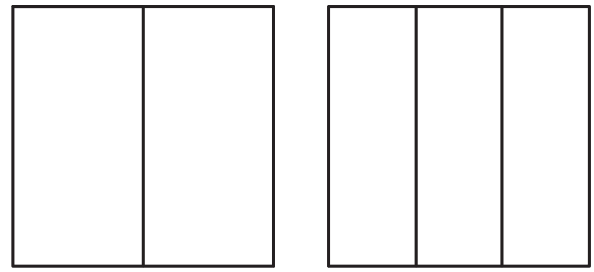

Fig. 1. Double-cell and triple-cell sections studied by Chen and Wierzbicki [11].

$$MCF = 13.06\sigma_0 b^{\frac{1}{3}}t^{\frac{5}{3}} \tag{4}$$

Where σ_0 is the flow stress of the material, t denotes the wall thickness and b means the sectional width. The flow stress σ_0 is not a constant value because of the strain hardening effects of the material. In this paper, σ_0 is obtained as the average of the yield strength σ_y and the ultimate strength σ_u of the material [14].

Chen and Wierzbicki [11] used a simplified method to apply the Super Folding Element theory [20] to predict MCF of double-cell and triple-cell tubes, as shown in Fig. 1. The formula can be written in Eq. (5).

$$MCF = \frac{2}{3}\sigma_0 t\sqrt{\pi NA} \tag{5}$$

where A is area of the section and N means the number of contributing flange.

Zhang et al. [12] proposed a formula (Eq. (6)) for predicting MCF by calculating energy absorbed through deformation of three kinds of elements, namely corner, cross and T-shape elements (Fig. 2):

$$MCF = \sigma_0 t\sqrt{(N_c + 4N_o + 2N_T)\pi L_c t} \tag{6}$$

where N_c, N_o and N_T are amounts of corner elements, crisscross elements and T-shape elements respectively, and L_c means the total length of all flanges.

Alavinia et al. [15] improved Zhang's formula to calculate MCF of unequal multi-cell structure. Parameters involving Z_c, Z_o and Z_T were introduced as the ratios of the lengths of corner, crisscross and T-shape elements in equal multi-cell section to the lengths of these elements in unequal multi-cell section (Fig. 3).

Ratios are defined as

$$Z_c = \frac{S_c}{P_c},\ Z_o = \frac{S_o}{P_o},\ Z_T = \frac{S_T}{P_T} \tag{7}$$

Eq. (8) is the revised version of Eq. (6), therefore, MCF of unequal multi-cell tubes is calculated by Eq. (8).

$$MCF = \sigma_0 t\sqrt{\left(\left(\frac{3a}{L}\right)N_c + 6\left(\frac{L-a}{L}\right)N_o + 2N_T\right)\pi L_c t} \tag{8}$$

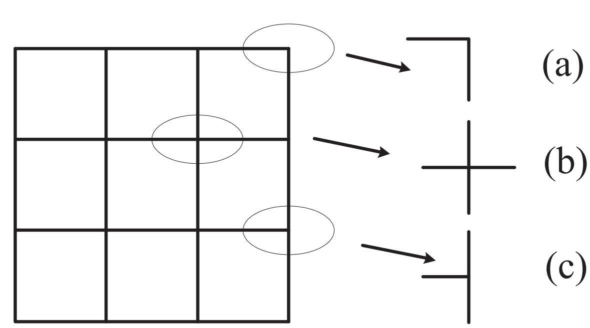

Fig. 2. (a) Corner element, (b) Crisscross element, (c) T-shape element [12].

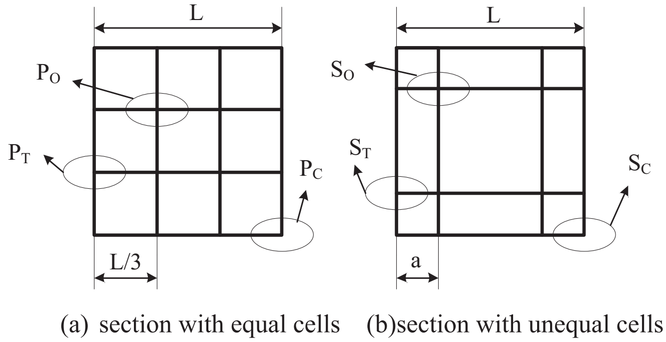

Fig. 3. 3 × 3 square section by Alavinia et al. [15]. (a) Section with equal cells (b)section with unequal cells.

3.2. Improved formula for predicting MCF

Eqs. (4)–(6) and (8) have been validated to determine MCF of tubes with multi-cell sections with high accuracy [11,12,15,21,22]. However, Eqs. (6) and (8) were derived for only square tubes and could not be used directly for predicting MCF of rectangular columns. In this work, an improved formula based on Eq. (8) is derived for calculate MCF of rectangular unequal triple-cell tubes which contains four corner elements and four T-shape elements (Fig. 4(c)). Based on Eqs. (7) and (8), MCF of unequal rectangular triple-cell (Fig. 4(c)) tube can be calculated by Eq. (9):

$$MCF = \sigma_0 t_3 \sqrt{\left(3\left(\frac{b_3 + d}{a_3 + 3b_3}\right)N_c + 6\left(\frac{a_3 + b_3 - d}{2a_3 + 3b_3}\right)N_o\right)\pi L_c t_3} \tag{9}$$

4. Simulations and experimental validation

4.1. Geometrical parameters and material properties

In experiments and simulations, rectangular tubes of single-cell, double-cell and unequal triple-cell sections were fabricated and constructed. Fig. 4 and Table 1 show geometrical parameters of specimens. Samples are all made of aluminum alloy 6106-T7 whose mechanical properties are listed in Table 2. The height of tubes was all selected to be 300 mm. In addition, another type of triple-cell tube with the length of 385 mm was chosen to investigate the effects on energy absorption in terms of different heights.

4.2. Numerical modeling

Numerical models are constructed using the explicit FE code LS-DYNA with the same sizes and material properties in experiments. All four models are meshed by four-node Belytschko-tsay thin shell elements. The element size is chosen as 2 mm and therefore, the shell element numbers are 21,900 for the single-cell model, 27,000 for the double-cell model, 33,000 for the triple-cell model (300 mm) and 42,460 for the triple-cell model (385 mm). A typical model consists of three main parts, namely the upper rigid wall, the tube body and the lower fixed wall. The materials of two walls and the tube are defined using MAT 20 rigid material and MAT 24 piecewise linear plasticity material respectively. In the respect of boundary conditions, all degrees of freedom of fixed wall are constrained and the lower end of the tube is fully attached to lower fixed wall. By applying axial load and a constant velocity of 50 mm/min, the upper rigid wall moves downwards to crush the tube, and the tube body is compressed with a final deformation of 70% of its total length. In terms of contact settings, the automatic node to surface algorithm is employed as the contact between the upper rigid wall and the tube body with a friction coefficient of $\mu = 0.2$. Another automatic single surface algorithm is applied to avoid interpenetration in the tube. A typical model is described in Fig. 5(b).

Table 1
Geometrical parameters of specimens.

i	a_i (mm)	b_i (mm)	t_i (mm)	d (mm)
1	80	70	2.2	–
2	88	70	2.2	–
3	110	60	2.2	22

Table 2
Aluminum alloy 6106-T7.

Young's modulus	Poisson's ratio	Yield stress	Ultimate stress
71.78 MPa	0.33	109 MPa	191 MPa

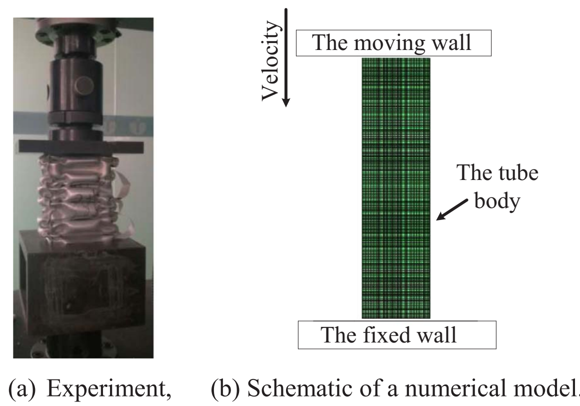

Fig. 5. Experiment and description of a model in simulations. (a) Experiment, (b) Schematic of a numerical model.

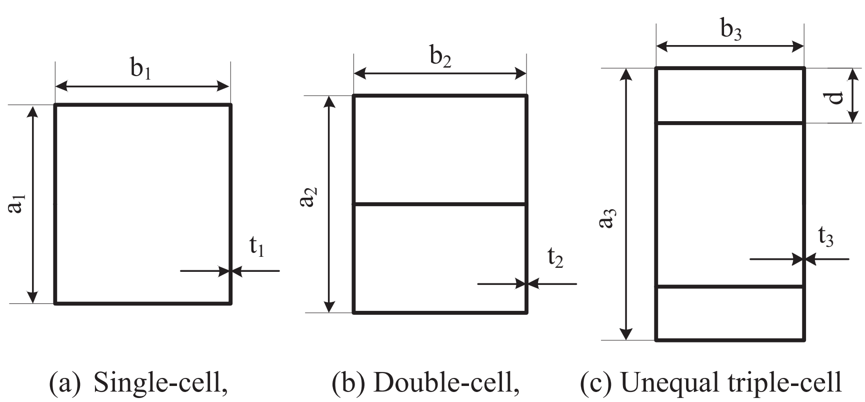

Fig. 4. Geometrical parameters of cross sections. (a) Single-cell, (b) Double-cell, (c) Unequal triple-cell.

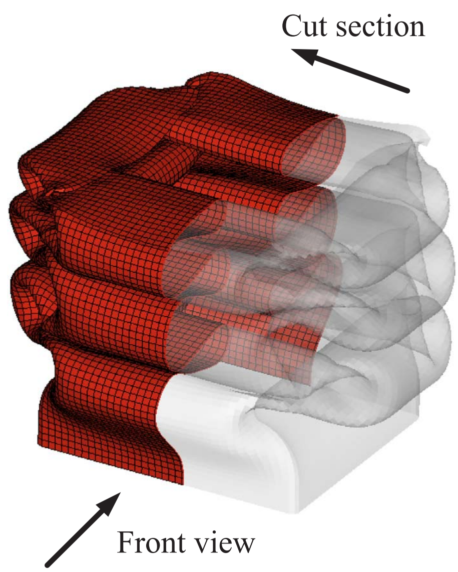

Fig. 6. View orientations of a crushed tube.

4.3. Results discussion

To verify whether the numerical results reflect crushing experiments accurately, results obtained from simulations are validated against experimental data. Fig. 6 illustrates a typical deformation pattern of the tube and gives two points of view to better observe the external and internal deformation. One of views is the front view and another is the cut section that is perpendicular to the front view. Fig. 7 compares deformation patterns in experiments and two views from simulations. It can be clearly noticed that all samples developed the progressive crushing mode. The deformation pattern and the number of folds in simulations show great agreement with those in experiments.

MCF-Displacement line graphs are plotted in Fig. 8. Fig. 8(a)–(d) compare these curves from experiments, simulations and predictions for different sectional configurations respectively; (e) and (f) compare these curves of three different cross sections. The criteria values obtained from experiments, simulations and predictions are summarized in Table 3. The MCF predictions of single- and double-cell are calculated by Eqs. (4) and (5), those of triple-cell tubes are obtained using Eq. (9). It can be clearly observed that curves in both simulations and experiments have the similar trend that, after reaching peaks, force drops and fluctuates around the mean figures. From Table 3, Fig. 8(c) and (d), it can be noticed that two kinds triple-cell tube of different

Fig. 7. Comparison of deformation patterns in experiments and simulations. (a) Single-cell, (b) Double-cell, (c) Triple-cell (300 mm), (d) Triple-cell (385 mm).

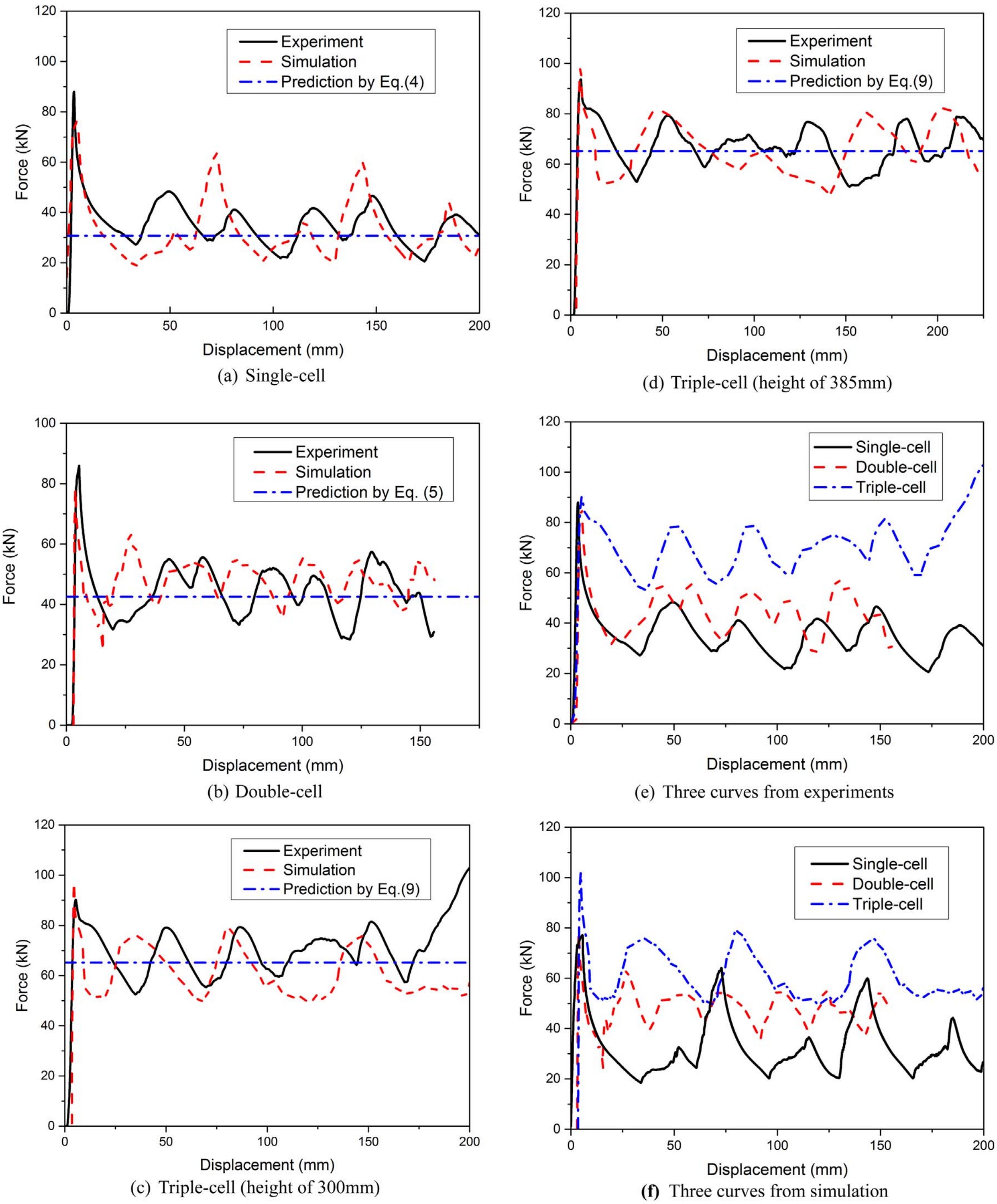

Fig. 8. Comparison of Force-Displacement curves. (a) Single-cell, (b) Double-cell, (c) Triple-cell (height of 300 mm), (d) Triple-cell (height of 385 mm), (e) Three curves from experiments, (f) Three curves from simulation.

lengths have the same crushing mode, similar analytical and experimental results. Therefore, the axial lengths' effects on crashworthiness are not obvious and can be ignored in engineering fields. According to Fig. 8 and Table 3, triple-cell tubes have the highest MCF, CFE and SEA, followed by double-cell and single-cell tubes successively. It can be summarized that triple-cell tube exhibits the best crashing performance among all tubes. In addition, results from simulations, experiments and theoretical verifications show good correspondence, therefore, it can be concluded that numerical models in this study are sufficiently accurate and can be used in further optimization design.

5. Optimization design for unequal triple-cell tube

In many cases, due to car body layouts and assembling requirements, engineers design metal absorbers under certain external dimensions. Therefore, it is necessary to find proper wall thicknesses and internal arrangements to realize the best crashworthiness. The task of finding the optimal design under certain conditions calls for optimization design. In this study, multi-objective optimization method is introduced to find an optimal solution to this problem.

Table 3
Results of experiments, prediction and simulations.

		MCF (kN)	CFE	SEA (J/g)
Single-cell	Experiment	35.22	0.40	14.02
	Simulation	33.21	0.43	13.02
	Prediction	30.74	–	–
Double-cell	Experiment	44.55	0.52	15.40
	Simulation	48.25	0.59	15.56
	Prediction	42.53	–	–
Triple-cell (300 mm)	Experiment	68.22	0.74	16.13
	Simulation	67.04	0.64	16.29
	Prediction	65.18	–	–
Triple-cell (385 mm)	Experiment	67.18	0.72	15.98
	Simulation	65.23	0.70	15.95
	Prediction	65.18	–	–

Table 4
The initial designs and targets of objectives.

Objectives	Initial value	Target
SEA $f_1(t,d)$	16.29 J/g	Maximize
MCF $f_2(t,d)$	68.22 kN	Minimize

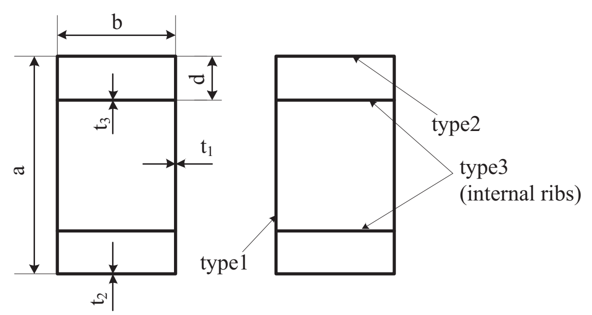

Fig. 9. Optimization design parameters.

Table 5
The initial designs and ranges of variables.

Variable	Initial design	Lower bound	Upper bound
t_1	2.2	2.0	3.0
t_2	2.2	2.0	3.0
t_3	2.2	2.0	3.0
d	22.0	10.0	50.0

5.1. Design objectives and variables

Crashworthiness design aims to maximize energy absorption when impact occurs. Note that increase in energy absorption always results in unwished increase in weight, and this is the reason why the SEA is presented to evaluate crashworthiness which takes both energy absorption and weight into account. Moreover, the MCF is an important criterion in crashworthiness design that indicates extent of impact when collision occurs. In this paper, maximization of SEA and minimization of MCF are selected as two objectives to be optimized in a multi-objective optimization framework. The initial values and targets of objectives are listed in Table 4.

Cross profile of a rectangular triple-cell tube is shown in Fig. 9. From the perspective of geometry, a column axially comprises of six planar plates which can be classified into three types when considering structural symmetry (Fig. 9). In order to explore how different thicknesses of each type of plate lead to different crashworthiness, three thicknesses are chosen as variables in optimization design as shown in Fig. 9. In addition, one type of plates is the two internal ribs pointed out in Fig. 9, and the location of internal ribs determines the layout of cells which influence crashworthiness prominently [15]. Therefore, another variable d (Fig. 9) is chosen in the optimization framework. Table 5 lists initial designs and ranges for all variables. In this optimization design, the length (a in Fig. 9), width (b in Fig. 9) and height of the tube are set as 110 mm, 60 mm and 300 mm respectively, the same in experiments and simulations.

The general optimization problem for crashworthiness of rectangular unequal triple-cell tube is defined as:

$$\begin{aligned} &\text{Minimize} \quad [-f_1(t, d),\ f_2(t, d)] \\ &\text{Subject to} \quad t^{L} \le t_i \le t^{U} \quad i = 1, 2, 3 \\ &\qquad\qquad\quad d^{L} \le d \le d^{U} \end{aligned} \tag{10}$$

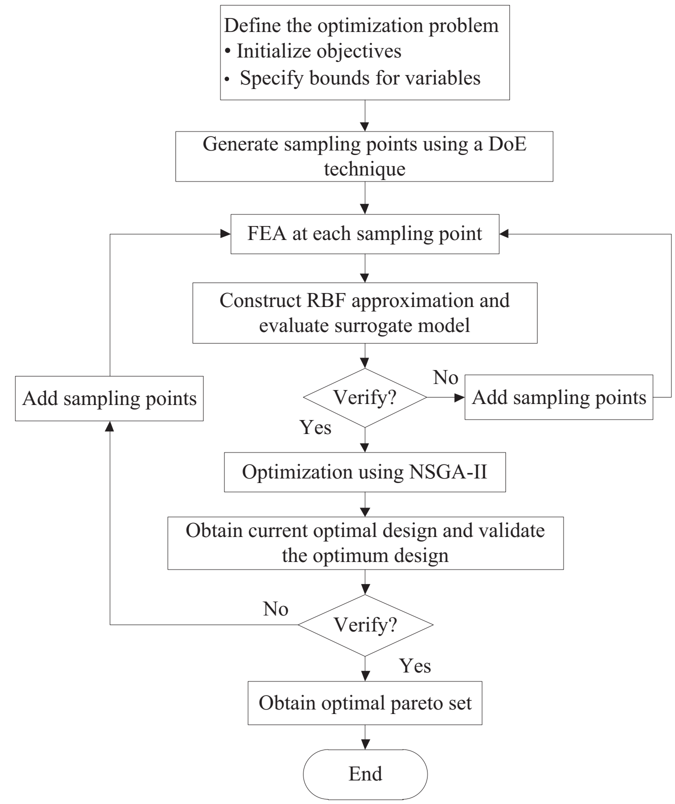

Fig. 10. Flowchart of the optimization procedure.

Table 6
Accuracy evaluation.

Objectives	max(RE)	R^2	RMSE
MCF	4.08%	0.93	0.08
SEA	3.12%	0.95	0.06

Table 7
Parameters for NSGA-II algorithm.

Parameters	Value
Population size	20.0
Number of generations	50.0
Crossover probability	0.9
Crossover distribution index	10.0
Mutation distribution index	20.0

5.2. Optimization procedure

The flowchart of the optimization design is described in Fig. 10. At the first stage of the process, two objectives and four variables are

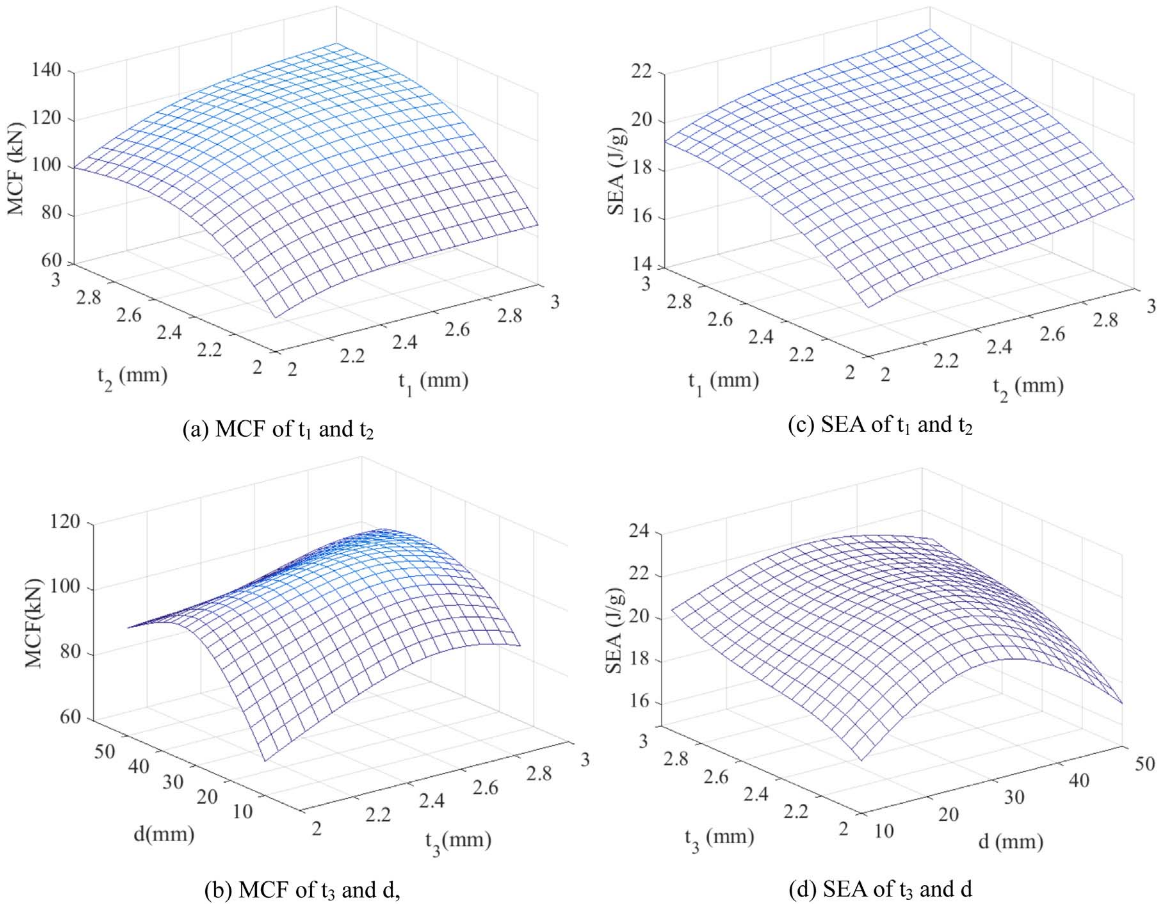

Fig. 11. Surrogate model for optimization (a) MCF of t_1 and t_2, (b) MCF of t_3 and d, (c) SEA of t_1 and t_2, (d) SEA of t_3 and d.

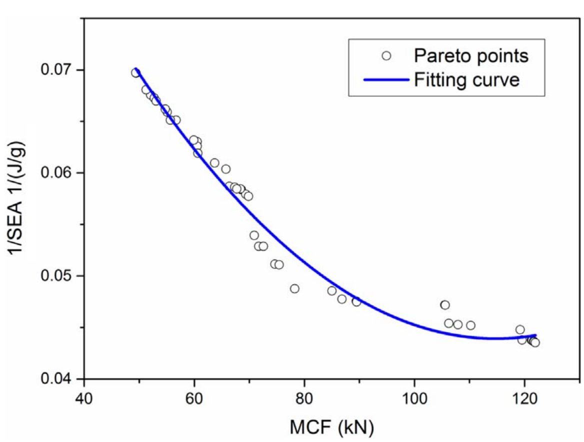

Fig. 12. Pareto frontier for optimization.

Table 8
Optimization results.

t_1 (mm)	t_2 (mm)	t_3 (mm)	d (mm)
2.00	2.04	2.86	26.93

Table 9
Comparison between optimization results and FE values.

Objectives	Optimization	FE	Error
SEA	19.23	19.65	2.18%
MCF	71.08	69.89	1.67%

Table 10
Optimum values versus initial design of triple-cell tube.

Objectives	Initial model	Optimum model	Improvement
SEA(J/g)	16.29	19.65	3.36
MCF(kN)	68.22	69.89	−1.87

defined in line with actual demand in engineering. The optimal Latin hypercube sampling technique (OLHS) is then employed as DoE sampling method for variables and 40 design sampling points are generated in this optimization. At the following stage, the finite element analysis (FEA) is conducted to obtain objective values for every sampling point using LS-DYNA. It should be noted that SEA and MCF are non-linear functions to design variables, the radial basis function (RBF) is chosen to construct metamodel in this study since RBF technique has proven accurate in highly nonlinear problems [23–25].

To estimate the fitting accuracy of approximate model, max(RE), Coefficient of determination (R^2) and root mean square error (RMSE) are selected as criteria [13]. RE is often adopted to measure the degree of approximation to the FEA results; R^2 and RMSE are typical statistical parameters used for assessing fitness of surrogate models. These three criteria are defined mathematically as

$$RE = \left| \frac{y_i - \hat{y}_i}{y_i} \right| \tag{11}$$

$$R^2 = 1 - \frac{\sum_{i=1}^{n} (y_i - \hat{y}_i)^2}{\sum_{i=q}^{n} (y_i - \hat{y}_i)^2} \tag{12}$$

$$RMSE = \sqrt{\frac{\sum_{i=1}^{n}(y_i - \bar{y}_i)^2}{\sum_{i=1}^{n}\bar{y}_i}} \quad (13)$$

where y_i is the simulation value for each sampling point; $\hat{y}_i$ the predicted value; $\bar{y}_i$ the mean value of y_i. For an accurate approximate model, it is preferable to have RE and RMSE to be nearly close to 0 and R^2 to 1. Because sampling points abovementioned for model construction can not be used in evaluation, additional 10 validation points are generated to assess the accuracy of surrogate model. After evaluation, when these criteria all reach requirements, it can be said that the initial model is reasonably accurate. If criteria do not meet standard values, several other sampling points need to be generated to reconstruct the surrogate model.

Table 6 lists max(RE), R^2 and RMSE of MCF and SEA for validation points. It can be found that max(RE) is less than 5%, R^2 is more than 0.9 and RMSE is less than 0.1, indicating the RBF surrogate constructed in this study is sufficiently accurate for following optimizer.

Finally, Non-dominated Sorting Genetic algorithm (NSGA-II) is adopted in optimization based on the existing RBF model. The relevant NSGA-II parameters are listed in Table 7.

In multiobjective optimization design, the improvement of one objective is always at the sacrifice of another, and vice versa - that is to say, objectives are in conflict with each other. Because of this, Pareto frontier contains a set of values and any point in Pareto set can be a solution to the optimization problem. In most cases, it is necessary to select the most satisfactory solution from the Pareto set, namely the knee point, which has the shortest distance from the utopia point. In this paper, Deb and Gupta's [26] method is employed to define the knee point.

According to Table 6, the initial RBF model has reasonable accuracy in terms of max(RE), R^2 and RMSE, but it cannot be guaranteed to obtain high accurate optimization results using the fixed surrogate model. Therefore, the RBF model is updated in an iterative manner till satisfactory optimal results are obtained. To verify the fitness of Pareto results, the FEA is performed at the current optimal solution and another two randomly selected points. The errors are evaluated by relative error (RE) (Eq. (11)). If the any RE exceeds a certain tolerance, e.g. 5%, additional sampling points need to be added and the RBF model should be rebuilt. The circle will terminate when all the REs are below the tolerance threshold, which indicates that the surrogate model is reliable and can be applied in following optimization.

5.3. Results of optimization

Fig. 11 shows the RBF approximate model, and from these surface graphs, the following information can be derived:

(1) SEA and MCF behave monotonically over the design domain of t_1, t_2 and t_3, which means that with the increase of t_1, t_2 and t_3, the SEA and MCF of tubes also rise;
(2) The d has the nonmonotonic surfaces in regards to SEA and MCF. It appears that SEA and MCF will reach their maximum values when d is around 30 mm.

Fig. 12 illustrates the Pareto frontier obtained from optimization procedure. It can be clearly observed that the two objectives strongly compete with each other and it is necessary to have a tradeoff to find a relatively optimal solution. Table 8 lists optimal design obtained from Pareto frontier. Compared with initial design shown in Table 5, t_1 and t_2 are close to the lower bound while t_3 approaches the upper bound, d increases from 22 mm to 26.93 mm.

To validate the optimization results, the numerical model for this optimal design is built in FE code LS-DYNA. Results of the numerical model and the optimization design are compared in Table 9, the relative errors between simulation and optimization values are less than 5% which signifies the optimization design is sufficiently accurate and can be accepted in engineering field.

Table 10 summarizes MCF and SEA of numerical results from initial model and the optimum design. It can be seen that there are a prominent improvement of 20.63% (from 16.29 J/g to 19.65 J/g) in SEA and a few sacrifices of 2.45% in MCF which is minimal and can be ignored in engineering.

6. Conclusion

This study investigated crashworthiness of rectangular single-, double- and unequal triple-cell tubes which were made of aluminum alloy. An analytical formula for predicting MCF of unequal triple-cell tubes was derivated first. Quasi-static crushing experiments and FEA were then conducted in axial direction for these three different tubes. The results from numerical simulation were compared well with data from experimental tests and theoretical predictions. It was found that the triple-cell tube exhibited the best crashing performance, followed by double- and single-cell counterparts. At the following stage, the multi-objective optimization design was carried out to investigate the effect of the thickness of each plate and arrangements of internal ribs on SEA and MCF. RBF technique and NSGA-II were applied in this optimization. According to optimization results, it could be observed that there were noticeable improvements in SEA with a few sacrifices in MCF, which was acceptable in engineering field. More importantly, this optimization provided an idea that when designing similar structures, increasing the thicknesses of internal ribs while decreasing thicknesses of outside plates could lead to better crashworthiness to some extent.

Acknowledgments

This work is supported jointly by National Natural Science Foundation of China (No. 51405123), the Open Fund of Key Laboratory of Advanced Manufacture Technology for Automobile Parts (Chongqing University of Technology), Ministry of Education of China (No. 2014KLMT03) and the Open Fund of Zhejiang Key Laboratory of Automobile Safety Technology (No. 2009E10013).

References

[1] V. Jandaghishahi, J. Marzbanrad, Analytical and experimental studies of quasi-static axial crush behavior of thin-walled tailor-made aluminum tubes, Thin-walled Struct. 60 (2012) 24–37.
[2] T.N. Tran, S. Hou, X. Han, W. Tan, N.T. Nguyen, Theoretical prediction and crashworthiness optimization of multi-cell triangular tubes, Thin-Walled Struct. 82 (2014) 183–195.
[3] M. Dass Goel, Deformation absorption and crushing behavior of single-, double- and multi-wall foam filled square and circular tubes, Thin-Walled Struct. 90 (2015) 1–11.
[4] A. Alavinia, S. Chahardoli, Optimizing the layout of nested three-tube structures in quasi-static axial aollapse, Thin-Walled Struct. 107 (2016) 169–181.
[5] S. Salehghaffari, M. Tajdari, M. Panahi, F. Mokhtarnezhad, Attempts to improve energy absorption characteristics of circular metal tubes subjected to axial loading, Thin-Walled Struct. 48 (2010) 379–390.
[6] G. Sun, F. Xu, G. Li, Q. Li, Crashing analysis and multiobjective optimization for thin-walled structure with functionally graded thickness, Int. J. Impact Eng. 64 (2014) 62–74.
[7] S. Hou, Q. Li, S. Long, X. Yang, W. Li, Design optimization of regular hexagonal thin-walled columns with crashworthiness criteria, Finite Elem. Anal. Des. 43 (2007) 555–565.
[8] A. Ghamarian, H. Zarei, Crashworthiness investigation of conical and cylingdrical end-capped tubes under quasi-static crash loading, Int. J. Crashworthiness 17 (2012) 19–28.
[9] C. Qi, S. Yang, F. Dong, Crushing analysis and multiobjective crashworthiness optimization of tapered square tubes under oblique impact loading, Thin-Walled Struct. 59 (2012) 103–119.
[10] H.R. Zarei, M. Kroger, Multiobjective crashworthiness optimization of circular aluminum tubes, Thin-Walled Struct. 44 (2006) 301–308.
[11] W. Chen, T. Wierzbicki, Relative merits of single-cell, multi-cell and foam-filled thin-walled structure in energy absorption, Thin-Walled Struct. 39 (2001) 287–306.
[12] X. Zhang, G. Cheng, H. Zhang, Theoretical prediction and numerical simulation of multi-cell square thin-walled structures, Thin-Walled Struct. 44 (2006) 1185–1191.
[13] S. Hou, Q. Li, S. Long, X. Yang, W. Li, Multiobjective optimization of multi-cell

sections for the crashworthiness design, Int. J. Impact Eng. 35 (2008) 1355–1367.
[14] X. Zhang, H. Zhang, Energy absorption of multi-cell stub columns under axial compression, Thin-Walled Struct. 68 (2013) 156–163.
[15] A. Alavinia, M. Parsapour, An investigation on the energy absorption characteristics of multi-cell square tubes, Thin-Walled Struct. 68 (2013) 26–34.
[16] G. Sun, G. Li, S. Zhou, H. Li, S. Hou, Q. Li, Crashworthiness design of vehicle by using multiobjective robust optimization, Struct. Multidiscip. Optim. 44 (2011) 99–110.
[17] X. Gu, G. Sun, G. Li, A comparative study on multiobjective reliable and robust optimization for crashworthiness design of vehicle structure, Struct. Multidiscip. Optim. 48 (2013) 669–684.
[18] X. Gu, G. Sun, G. Li, Multiobjective optimization design for vehicle occupant restraint system under frontal impact, Struct. Multidiscip. Optim. 47 (2013) 465–477.
[19] S. Hou, T. Liu, D. Dong, X. Han, Factor screening and multivariable crashworthiness optimization for vehicle side impact by factorial design, Struct. Multidiscip. Optim. 49 (2014) 147–167.
[20] M. Costas, J. Diaz, L. Romera, S. Hernandez, A multi-objective surrogate-based optimization of the crashworthiness of a hybrid impact absorber, Int. J. Mech. Sci. 88 (2014) 46–54.
[21] T. Wierzbicki, W. Abramowicz, On the crushing mechanics of thin-walled structures, J. Appl. Mech. 50 (1983) 727–739.
[22] W. Abramowicz, T. Wierzbicki, Axial crushing of multi-corner sheet metal columns, J. Appl. Mech. 56 (1) (1989) 113–120.
[23] H. Yin, G. Wen, Z. Liu, Q. Qing, Crashworthiness optimization design for foam-filled multi-cell Thin-walled structures, Thin-Walled Struct. 75 (2014) 8–17.
[24] E. Acar, M.A. Gular, B. Gerceker, M.E. Ceit, B. Bayram, Multi-objecctive crashworthiness optimization of tapered thin-walled tubes with axisymmetric indentations, Thin-Walled Struct. 49 (2011) 94–105.
[25] G. Li, Z. Zhang, G. Sun, X. Huang, Q. Li, Comparison of functionally-graded structures under multiple loading angles, Thin-Walled Struct. 94 (2015) 334–347.
[26] K. Deb, S. Gupta, Understanding knee points in bacriteria problems and their implications as preferred solution principles, Eng. Optim. 43 (2011) 1175–1204.